BJP British Journal of Pharmacology

DOI:10.1111/bph.13079
www.brjpharmacol.org

RESEARCH PAPER

Glucose modulation induces reactive oxygen species and increases P-glycoprotein-mediated multidrug resistance to chemotherapeutics

N A Seebacher, D R Richardson* and P J Jansson*

Molecular Pharmacology and Pathology Program, Department of Pathology and Bosch Institute, Blackburn Building (D06), University of Sydney, Sydney, NSW, Australia

Correspondence
Patric J Jansson and Des R Richardson, University of Sydney, Sydney, New South Wales, Australia. E-mail: patric.jansson@sydney.edu.au; d.richardson@sydney.edu.au

*Contributed equally to the work as co-corresponding and senior authors.

Received
22 September 2014
Revised
8 December 2014
Accepted
5 January 2015

BACKGROUND AND PURPOSE

Cancer cells develop resistance to stress induced by chemotherapy. In tumours, a considerable glucose gradient exists, resulting in stress. Notably, hypoxia-inducible factor-1 (HIF-1) is a redox-sensitive transcription factor that regulates P-glycoprotein (Pgp), a crucial drug-efflux transporter involved in multidrug resistance (MDR). Here, we investigated how glucose levels regulate Pgp-mediated drug transport and resistance.

EXPERIMENTAL APPROACH

Human tumour cells (KB31, KBV1, A549 and DMS-53) were incubated under glucose starvation to hyperglycaemic conditions. Flow cytometry assessed reactive oxygen species (ROS) generation and Pgp activity. HIF-1α, NF-κB and Pgp expression were assessed by reverse transcriptase-PCR and Western blotting. Fluorescence microscopy examined p65 distribution and a luciferase-reporter assay assessed *HIF-1* promoter-binding activity. The effect of glucose-induced stress on Pgp-mediated drug resistance was examined after incubating cells with the chemotherapeutic and Pgp substrate, doxorubicin (DOX), and performing MTT assays validated by viable cell counts.

KEY RESULTS

Changes in glucose levels markedly enhanced cellular ROS and conferred Pgp-mediated drug resistance. Low and high glucose levels increased (i) ROS generation *via* NADPH oxidase 4 and mitochondrial membrane destabilization; (ii) HIF-1 activity; (iii) nuclear translocation of the NF-κB p65 subunit; and (iv) *HIF-1α* mRNA and protein levels. Increased HIF-1α could also be due to decreased prolyl hydroxylase protein under these conditions. The HIF-1α target, Pgp, was up-regulated at low and high glucose levels, which led to lower cellular accumulation of Pgp substrate, rhodamine123, and greater resistance to DOX.

CONCLUSIONS AND IMPLICATIONS

As tumour cells become glucose-deprived or exposed to high glucose levels, this increases stress, leading to a more aggressive MDR phenotype *via* up-regulation of Pgp.

Abbreviations

ABC, ATP-binding cassette; AM, antimycin A; DOX, doxorubicin; Ela, Elacridar; DCF, 2′,7′-dichlorofluorescein; H_2DCF, 2′,7′-dichlorodihydrofluorescein; H_2DCFDA, 2′,7′-dichlorodihydrofluorescein diacetate; HIF-1, hypoxia-inducible factor-1; MDR, multidrug resistance; NOX, NADPH oxidase; PEG-SOD, superoxide dismutase–polyethylene glycol; Pgp, P-glycoprotein; PHD2, prolyl hydroxylase 2; Rh123, rhodamine123; ROS, reactive oxygen species; VBL, vinblastine

Tables of Links

TARGETS	
Transporters[a]	**Enzymes**[b]
ABCG2	HDAC1
GLUT1	**Other protein targets**
MRP1 (ABCC1)	VEGFA
P-glycoprotein (ABCB1; MDR1)	

LIGANDS	
ATP	H_2O_2
D-glucose	Pyruvate
Doxorubicin (DOX)	Rhodamine123
Glutamine	Vinblastine
Glutathione	

These Tables list key protein targets and ligands in this article which are hyperlinked to corresponding entries in http://www.guidetopharmacology.org, the common portal for data from the IUPHAR/BPS Guide to PHARMACOLOGY (Pawson *et al.*, 2014) and are permanently archived in the Concise Guide to PHARMACOLOGY 2013/14 ([a,b]Alexander *et al.*, 2013a,b).

Introduction

The intracellular glucose concentration markedly depends on glucose uptake, cellular metabolism and the concentration of extracellular glucose (Prochazkova *et al.*, 2011). Malignant cells display enhanced glycolysis as a result of their accelerated metabolism, high glucose requirements and increased glucose uptake (Chen and Russo, 2012). As a consequence of the increased reliance on aerobic glycolysis, as well as vascularization and elevated proliferation, there exists a considerable glucose-gradient within tumours (Chaplain, 1996; Pelicano *et al.*, 2006; Annibaldi and Widmann, 2010). This microenvironment exposes a significant portion of cancer cells to extremely low or high glucose concentrations (Casciari *et al.*, 1988; Walenta *et al.*, 2002; Yeom *et al.*, 2012). Moreover, studies have associated increased reactive oxygen species (ROS) with conditions of excess and limited glucose (Yu *et al.*, 2011; Graham *et al.*, 2012).

Previous studies have demonstrated that intracellular ROS are primarily formed *via* NADPH oxidases (NOX) or as a by-product of the electron-transport chain (Murphy, 2009; Block and Gorin, 2012). While ROS can mediate cytotoxicity, there is also evidence to support their role in signal transduction (Behrend *et al.*, 2003). Furthermore, ROS can modulate transcription factor activity, including hypoxia-inducible factor-1 (HIF-1) and NF-κB (Denko, 2008; Hagen, 2012). These transcription factors have been linked to increased expression of the ATP-dependent, drug-efflux 'pump', P-glycoprotein (Pgp) (Milane *et al.*, 2011). This transmembrane protein is the most consistently overexpressed ATP-binding cassette (ABC) transporter involved in multidrug resistance (MDR), which represents a major concern to successful chemotherapeutic treatment (Longley and Johnston, 2005; Milane *et al.*, 2011).

This study aimed to establish the relationship between stress induced by the tumour cell microenvironment and modulation of the drug-resistant phenotype, using a cell culture model. Herein, we report that variation in glucose levels confers Pgp-mediated drug resistance to the chemotherapeutic and Pgp substrate, doxorubicin (DOX). Low or high glucose levels, relative to standard culture conditions, induced oxidative stress, nuclear translocation of the NF-κB p65 subunit and increased HIF-1α-expression. This increase in HIF-1α was implicated in the increased Pgp expression, which leads to greater DOX resistance. These studies highlight how glucose-induced stress increases MDR in a tumour cell culture model.

Methods

Cell culture

The human DMS-53 small cell lung carcinoma cell line and the A549 non-small cell lung carcinoma cell lines were obtained from the American Type Culture Collection (Manassas, VA, USA). The human KB31 and KBV1 cervical carcinoma cell lines were from Dr M. Kavallaris (Children's Cancer Institute Australia, NSW). Medium for growing KBV1 cells was supplemented with VBL (0.8 $\mu g \cdot mL^{-1}$) for maintenance of a partial MDR phenotype, allowing Pgp induction upon stimulation. All media were supplemented with penicillin (100 $U \cdot mL^{-1}$), streptomycin (100 $mg \cdot mL^{-1}$), glutamine (2 mM), non-essential amino acids (100 mM) and pyruvate (100 mM; all from Life Technologies). Cells were maintained in DMEM ([D-glucose] = 25 mM; Life Technologies). At the time of treatment, media was replaced with glucose-free DMEM (-D-glucose, 0 mM) or this medium supplemented with D-glucose (final [glucose] = 12.5 or 50 mM).

For all experiments, to study glucose-induced stress, cells were exposed to either: (i) glucose-deprivation (0 mM); (ii) low glucose (12.5 mM); (iii) the glucose concentration used in DMEM (from the manufacturer) to routinely culture cells (25 mM; herein referred to as 'normal glucose'); or (iv) high glucose (50 mM) for 30 min/37°C. Preliminary studies demonstrated that because the cells were routinely cultured under standard growth medium using glucose at 25 mM, they had become accustomed to these conditions. Indeed, the higher and lower concentrations of glucose implemented were essential in order to observe the glucose-induced stress response. Hence, this culture model simulates the hypo- and hyperglycaemic conditions found *in vivo*. Studies were also performed in an attempt to adjust the cells to lower glucose concentrations (<20 mM) by prolonged incubations at these levels. However, these experiments were unsuccessful and led to a significant decrease in cellular viability (not shown).

Protein extraction and Western blotting

Whole cell, membrane protein extractions and Western blotting were performed using standard procedures (Zhong *et al.*, 2008; Saletta *et al.*, 2010). Nuclear/cytosolic extractions were achieved *via* the NE-PER nuclear cytoplasmic kit (ThermoFisher, VIC, Australia). GAPDH and histone deacetylase-1 (HDAC1) were used as controls for cytoplasmic and nuclear fractions respectively (Kovacevic *et al.*, 2013). H_2O_2 was used as it increases nuclear p65 localization (Takada *et al.*, 2003).

The role of ROS in this pathway was assessed by the utilization of the ROS scavenger and GSH-precursor, NAC (5 mM; De Flora *et al.*, 1995)], or the NOX inhibitor, apocynin (50 μM; Petronio *et al.*, 2013). NAC or apocynin were added before (30 min/37°C) and during the glucose treatment. H_2O_2 and the mitochondrial electron-transport chain inhibitor, AM (10 μM), were used as positive controls for the effects of ROS.

Membranes were probed using mouse anti-Pgp (Cat.#:P7965, 1:5000, Sigma-Aldrich), rabbit anti-GLUT1 (Cat.#:SAB4502803, 1:1000, Sigma-Aldrich); mouse anti-HIF-1α (Cat.#:610959, 1:400, BD Biosciences, San Jose, CA, USA); rabbit anti-prolyl hydroxylase 2 (PHD2; Cat.#:ab4561, 1:1000, Abcam, Cambridge, UK), rabbit anti-GAPDH (Cat.#:ab9485; 1:1000, Abcam); mouse anti-HDAC (Cat.#:5356, 1:1000, Cell Signaling, Danvers, MA, USA); or rabbit anti-p65 XP® (Cat.#:8242, 1:1000, Cell Signaling). Incubations were performed overnight/4°C followed by appropriate secondary antibody [HRP-conjugated goat anti-mouse (Cat.#:A4416, 1:10,000, Sigma-Aldrich) and goat anti-rabbit (Cat.#:A6154, 1:10,000; from Sigma-Aldrich) for 1 h/room temperature. Membranes were developed with enhanced chemiluminescence reagent (Amersham Pharmacia Biotech, Amersham, UK) and visualized using a ChemDoc system (BioRAD, Hercules, CA, USA). Densitometry was performed using ImageLab Software (BioRAD). β-actin (Cat.#:A5441; 1:500, Sigma-Aldrich) was used as a protein-loading control.

Cellular ROS assay

ROS were measured using the H_2DCFDA assay and detected using flow cytometry (FACSCanto™, BD Biosciences) at 488 nm excitation/530 nm emission. H_2DCFDA is de-acetylated by intracellular esterases to 2′,7′-dichlorodihydrofluorescein (H_2DCF) (Karlsson *et al.*, 2010). The H_2DCF directly detects hydroxyl radicals and indirectly detects superoxide and H_2O_2 as they become converted into hydroxyl radicals, which then oxidizes non-fluorescent H_2DCF to fluorescent DCF (Karlsson *et al.*, 2010). Hence, the DCF assay estimates total amount of intracellular ROS generated. Cells were incubated for 30 min/37°C with the Pgp inhibitor, Ela (0.2 μM), before the addition of the H_2DCFDA probe (25 μM; Life Technologies) to this medium for a further 30 min/37°C incubation. The medium was then replaced with glucose treatments (0–50 mM), and also Ela (0.2 μM) to prevent Pgp-dependent efflux of DCF (Prochazkova *et al.*, 2011). H_2O_2 (50 μM) was used as a positive control for DCF fluorescence, as shown previously (Keston and Brandt, 1965). Data were collected for 10 000 cells per sample and analysed using FlowJo software, version 7.5.5 (Tree Star, Inc., Ashland, OR, USA).

Transient NOX4-silencing

Cells were incubated for 6 h/37°C with an siRNA-Lipofectamine mixture (50 nM; *NOX4*-siRNA Cat.#:30141, Santa Cruz, CA, USA, and 1:200 Lipofectamine-2000, Life Technologies). This mixture was then replaced with media for a further 72 h/37°C before glucose treatments. The effectiveness of *NOX4* silencing was assessed using Western blotting. As a control, scrambled-siRNA (Scr-siRNA, Life Technologies) was used at the same concentration as *NOX4*-siRNA.

Mitochondrial ROS determination

Mitochondrial ROS were determined using the MitoSOX Red mitochondrial superoxide indicator (5 μM; Life Technologies). The incubation procedure was the same as that used for the H_2DCFDA probe and included the Pgp inhibitor, Ela (0.2 μM), to prevent probe efflux. Fluorescence intensity was measured using flow cytometry (FACSCanto, BD Biosciences) at 488 nm excitation/595 nm emission. Data were collected from 10 000 cells per sample and analysis performed using FlowJo software.

Mitochondrial membrane potential

Mitochondrial membrane potential was evaluated using the JC-1 probe (5,5′,6,6′–tetrachlor-1,1′,3,3′-tetraetylbenzimidazolylcarbocyanine iodide; Life Technologies). Cells were incubated for 30 min/37°C with glucose treatments in the presence or absence Ela (0.2 μM) to prevent Pgp-dependent probe efflux (Chaoui *et al.*, 2006). The JC-1 probe (10 μM) was then added to this medium for a further 15 min/37°C. The cells were then imaged using a confocal microscope (LSM 510 Meta; Zeiss, Oberkochen, Germany) and Axiovision software (Zeiss). Quantification of the red/green fluorescence was performed using ImageJ (NIH, Bethesda, MD, USA).

Pgp expression

Pgp expression was assessed by incubating cells with a FITC-conjugated Pgp antibody (Cat.#:557002, 1:5, BD Biosciences) for 30 min/37°C and detected using flow cytometry (FACSCanto, BD Biosciences) at 488 nm excitation/530 nm emission. Data were collected from 10 000 cells per sample. Data analysis was performed using FlowJo software.

Rh123 accumulation assay

Pgp functionality was assessed by measuring intracellular accumulation of the fluorescent Pgp substrate, Rh123 (Kawabata *et al.*, 1997). Cells were treated with glucose in the presence or absence NAC (5 mM). NAC was added before (30 min/37°C), and during the 24 h/37°C glucose treatment. After glucose treatments, cells were incubated with Rh123 (10 μM) for 30 min/37°C and analysed by flow cytometry (FACSCanto, BD Biosciences) at 510 nm excitation/595 nm emission. Data were collected from 10 000 cells per sample.

Immunofluorescence

Cells were fixed with paraformaldehyde (4%; 15 min/20°C) and permeabilized with digitonin (200 μM; 10 min/20°C). After blocking with 5% BSA, immunofluorescence was performed using a 16 h/4°C incubation with anti-NF-κB p65

Table 1
List of primer sets, expected product size and PCR programmes

Gene	Accession number	Species		Forward (5′ – 3′)	Product size	Program (temp/cycle)
MDR1	NM_000927.4	Human	F	TCACCAAGCGGCTCCGATACAT	1065	64/24
			R	CCCGGCTGTTGTCTCCATAGGC		
GLUT1	NM_006516.2	Human	F	CTTTGTGGCCTTCTTTGAAGT	168	58/24
			R	CCACACAGTTGCTCCACAT		
HIF-1α	NM_001530.3	Human	F	CTCGGCGAAGCAAAGAGT	578	56/38
			R	CAAGCACGTCATGGGTGG		
β-actin	NM_001101.3	Human	F	CCCGCCGCCAGCTCACCATGG	397	56/24
			R	AAGGTCTCAAACATGATCTGGGTC		

antibody (Cat.#:8242, 1:100, Cell Signaling), followed by an incubation of 16 h/4°C with an Alexa Fluor-conjugated secondary antibody (Cat.#:11012, 1:1000, Life Technologies). Images were captured with a confocal microscope (LSM 510 Meta; Zeiss) using green (495 nm excitation/516 nm emission) and red (577 nm excitation/592 nm emission) fluorescence.

RNA isolation and reverse transcriptase-PCR (RT-PCR)

Total RNA was isolated using TRIzol® (Life Technologies). RT-PCR was performed (Whitnall *et al.*, 2006) using the primers in Table 1. β-actin was used as an RNA-loading control. RT-PCR was shown to be semi-quantitative and in the log-phase of amplification.

HIF-1 promoter luciferase assay

Cells were transfected with a *HIF-1* promoter luciferase construct containing the mammalian *HIF-1* transcriptional regulatory-element sequence (5′-TACGTGCT-3′) (Wang and Semenza, 1993). Cells were also transfected with a constitutively expressing *Renilla* luciferase construct and a non-inducible Firefly luciferase construct, which acted as positive and negative controls, respectively, to validate transfection (see 'Positive' and 'Negative'). Luciferase assays were carried out using the Qiagen Luciferase Assay System (SAB Biosciences, VIC, Australia). Cells were transfected (24 h/37°C) before treatment. Protein extraction was performed using Luciferase Cell Culture Lysis Buffer (Promega, Madison, WI, USA). Luminescence was measured using a FLUOstar Omega Luminometer (BMG Labtech, VIC, Australia).

Proliferation assay

Cellular proliferation was assessed after drug treatments, in the presence or absence of a non-toxic concentration of Ela, using phase contrast microscopy and also MTT assays, which were validated by viable cell counts (Richardson *et al.*, 1995).

Data analysis

Results are expressed as mean ± SD ($n \geq 3$ experiments). Statistical analysis was performed using Student's *t*-test, with results being significant when $P < 0.05$. Concentration–response curves were fitted in Prism 6.0 (Graphpad Software, San Diego, CA, USA) to obtain IC_{50} values.

Chemicals

DOX was obtained from Pfizer (New York, NY, USA). 3-(4,5-Dimethyl-2-thiazolyl)-2,5-diphenyl-2H-tetrazolium bromide (MTT), superoxide dismutase–polyethylene glycol (PEG-SOD), apocynin, antimycin A (AM), H_2O_2, vinblastine (VBL), *N*-acetyl-L-cysteine (NAC) and rhodamine123 (Rh123) were purchased from Sigma-Aldrich (St. Louis, MO, USA). Elacridar (Ela; PSC833) was provided by GlaxoSmithKline (London, UK). MitoSOX™ and 2′,7′-dichlorodihydrofluorescein diacetate (H_2DCFDA) were from Life Technologies (Carlsbad, CA, USA).

Results

Multidrug-resistant cells are susceptible to glucose-induced ROS

Considering the link between glucose levels and cellular stress (Graham *et al.*, 2012), we assessed whether the well-characterized Pgp-expressing KBV1 cell line (Ludwig *et al.*, 2006) and their very low Pgp-expressing parental counterparts, namely KB31 cells (Figure 1A), were susceptible to glucose-induced stress.

Initially, we examined glucose-induced stress by assessing cellular ROS production, as measured by 2′,7′-dichlorofluorescein (DCF) fluorescence (Jansson *et al.*, 2010). For both cell types, an incubation for 30 min/37°C in media devoid of glucose (0 mM) resulted in significantly ($P < 0.001$–0.01) increased ROS levels as measured by DCF fluorescence relative to the normal glucose concentration (25 mM)

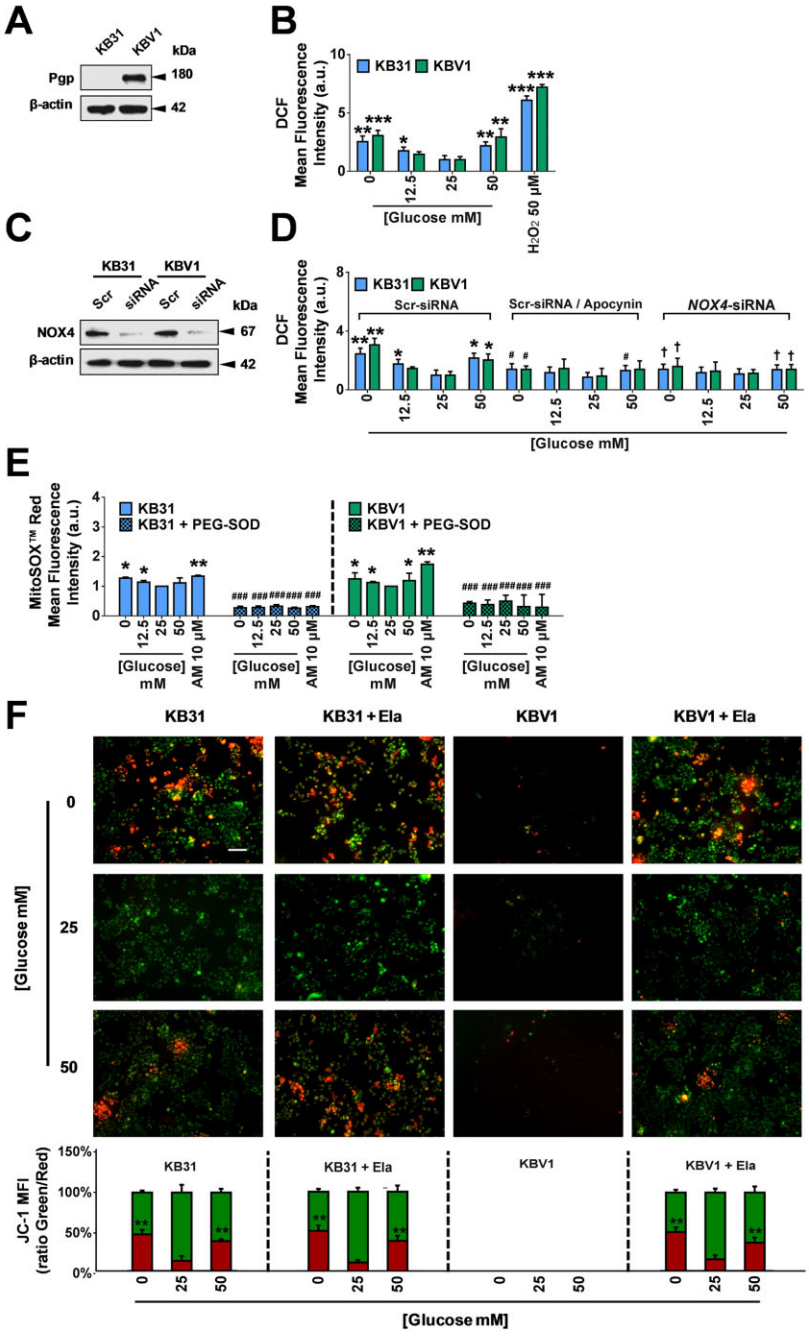

Figure 1

Changes in glucose levels lead to NOX4-mediated ROS generation, mitochondrial superoxide generation and mitochondrial membrane hyperpolarization (A) Western blot showing Pgp protein expression in KB31 and KBV1 cells. (B) Incubating KB31 and KBV1 cells for 30 min/37°C with low (0 and 12.5 mM) or high (50 mM) glucose compared with normal glucose (25 mM) increases DCF fluorescence. (C) Western blot showing NOX4 protein expression after silencing with *NOX4*-siRNA compared with Scr-siRNA-treated KB31 and KBV1 cells. (D) Incubation for 30 min/37°C with apocynin (50 µM), a NOX inhibitor, and transient silencing of NOX4, using *NOX4*-siRNA, decreases DCF fluorescence. (E) Mitochondrial superoxide production measured by MitoSOX Red (5 µM) increases after the glucose treatments in (B). Upon incubation of cells with PEG-SOD (1000 U·mL^{-1}) and the glucose treatments, MitoSOX was markedly decreased compared with the respective glucose treatments alone. (F) Increased red JC-1 fluorescence after a 30 min/37°C incubation with low (0 mM) or high (50 mM) glucose compared with normal glucose (25 mM). JC1 fluorescence was quantified and expressed as a ratio (red /green fluorescence. Data in (A, C) are typical blots from five experiments. Results in (B, D, E) are mean ± SD ($n = 5$). *$P < 0.05$, **$P < 0.01$, ***$P < 0.001$, versus control (25 mM glucose), $^{\#}P < 0.05$, $^{\#\#\#}P < 0.001$, $^{\dagger}P < 0.05$ versus respective glucose treatment alone in (D) Scr-siRNA cells, or (E) without PEG-SOD in KB31 or KBV1 cells. Data in (B, D, E) were normalized to the control (glucose; 25 mM) for both cell types. In (B, D, E), mean fluorescence intensity is presented as arbitrary units (a.u.). Immunofluorescence photographs in (F) are representative of three experiments and the quantified fluorescence intensity is presented as mean ± SD ($n = 3$). Scale bar: 50 µm.

(Figure 1B). At low glucose (12.5 mM), a slight, but significant ($P < 0.05$) increase in DCF fluorescence was observed with KB31 cells, but not KBV1 cells, relative to normal glucose (25 mM; Figure 1B). The high (50 mM) glucose concentration significantly ($P < 0.01$) elevated ROS generation compared with normal glucose (25 mM) in both cell lines (Figure 1B). The positive control, H_2O_2 (50 μM), significantly ($P < 0.001$) increased DCF fluorescence under normal glucose conditions in both cell types. Collectively, Pgp-expressing KBV1 and non-Pgp-expressing KB31 cells showed increased ROS generation in response to altered glucose levels. Studies then assessed the intracellular source of ROS production.

Mitochondrial NOX4 contributes to glucose-induced ROS production

The most abundant NOX4 is a major enzymatic generator of cellular H_2O_2 (Takac *et al.*, 2011), and was evaluated as a source of the redox-stress in Figure 1B in KB31 and KBV1 cells. To specifically assess the role of NOX4, the *NOX4*-isoform was silenced using siRNA and resulted in a significant ($P < 0.001$) 88 ± 4% decrease in NOX4 protein expression in both cell types relative to the respective Scr control (Figure 1C). Studies then assessed the effect of modulating glucose on ROS generation using these cells treated with Scr- and *NOX4*-siRNA, and also with the Scr-siRNA-treated cells incubated with the NOX inhibitor, apocynin (50 μM; Li *et al.*, 2010). In these experiments, cellular ROS generation was measured using the DCF assay (Figure 1D).

Upon modulation of glucose, KB31 (–Pgp) and KBV1 (+Pgp) cells incubated with Scr-siRNA responded in a similar way to their non-transfected counterparts (Figure 1B), with increased ROS being detected at low and high glucose levels relative to normal glucose (Figure 1D). The addition of the NOX inhibitor, apocynin, to Scr-siRNA-treated cells, resulted in a significant ($P < 0.05$) decrease in ROS generation following incubation with low glucose (0 mM in KB31 and KBV1 cells) and high glucose (50 mM in KB31 cells) relative to the respective Scr-siRNA glucose treatment (Figure 1D). Similarly, *NOX4*-siRNA significantly ($P < 0.05$) reduced ROS production at low (0 mM) and high (50 mM) glucose levels in both cell types, compared with the respective Scr-siRNA glucose treatment (Figure 1D). These results using apocynin or *NOX4*-siRNA indicated that NOX4 contributed to cellular ROS generation under glucose-induced stress conditions.

Modulation of media glucose concentration elevates mitochondrial electron-transport chain ROS production

Considering that inactivation of NOX activity or expression using apocynin or *NOX4*-siRNA, respectively, did not completely abolish ROS generation upon glucose modulation (Figure 1D), it was hypothesized that an additional, more limited source of redox-stress could also be involved. In fact, mitochondria produce a significant amount of ROS *via* the electron-transport chain (Nickel *et al.*, 2014), and this could be responsible. To assess this, the mitochondrial superoxide indicator, MitoSOX Red (Mukhopadhyay *et al.*, 2007), was used to measure mitochondrial superoxide, rather than H_2O_2 generated by NOX4 (Takac *et al.*, 2011). Notably, the low glucose (0 and 12.5 mM in KB31 and KBV1 cells) and high glucose levels (50 mM in KBV1 cells) significantly ($P < 0.05$) increased MitoSOX fluorescence compared with normal glucose (25 mM; Figure 1E). In these studies, the established electron-transport chain complex III inhibitor, AM (10 μM), was used as a positive control for induction of mitochondrial superoxide (Mattiazzi *et al.*, 2004), and significantly ($P < 0.01$) increased MitoSOX fluorescence compared with normal glucose (25 mM) in both cell types (Figure 1E).

As an additional control, the ROS scavenger, PEG-SOD (1000 U·mL^{-1}), a membrane-permeable antioxidant (Webb *et al.*, 1998), was used to inhibit ROS generation (Figure 1E). Incubation of KB31 (–Pgp) and KBV1 (+Pgp) cells with PEG-SOD for 30 min/37°C prior to, and during the 30 min/37°C glucose treatment, markedly and significantly ($P < 0.001$) reduced MitoSOX fluorescence for all glucose levels compared with their respective glucose treatment without PEG-SOD (Figure 1E). Together, these results in Figure 1D and E indicate that alterations in glucose levels increase ROS predominantly *via* NOX4-mediated H_2O_2 generation, but also through mitochondrial superoxide production.

Alteration in media glucose levels hyperpolarizes mitochondrial membranes

Hyperpolarization and depolarization of the mitochondrial membrane leads to ROS production that is triggered by an electron 'leak' from the mitochondrial respiratory chain (Wei and Dirksen, 2012), and may explain the results in Figure 1E. Using the well-characterized JC-1 probe, we examined the mitochondrial membrane potential as an indicator of mitochondrial dysfunction (Perelman *et al.*, 2012). Low mitochondrial inner-membrane potential leads to a green fluorescence with the JC-1 probe, while hyperpolarization increases JC1 red fluorescence (Perelman *et al.*, 2012). Significantly, experiments were performed in the presence or absence of the Pgp inhibitor, Ela (0.2 μM), to prevent Pgp-mediated efflux of JC-1 which is a Pgp substrate (Chaoui *et al.*, 2006).

Incubation of KB31 (–Pgp) cells with low (0 mM) or high (50 mM) glucose for 30 min/37°C resulted in a marked and significant ($P < 0.01$) increase in the ratio of red to green fluorescence compared with normal (25 mM) glucose-treated cells (Figure 1F). Similarly, significant ($P < 0.01$) alterations in fluorescence after glucose modulation were also observed for KB31 (–Pgp) cells in the presence of the Pgp inhibitor, Ela. In contrast, very few KBV1 (+Pgp) cells were fluorescent under the glucose treatments in the absence of Ela, with the fluorescence ratio not being calculated (Figure 1F). This occurred probably because the JC-1 probe was effectively effluxed out of these cells *via* Pgp (Chaoui *et al.*, 2006). However, in the presence of Ela, incubation of KBV1 (+Pgp) cells with low (0 mM) or high (50 mM) glucose resulted in a marked ($P < 0.01$) increase in red fluorescence compared with normal (25 mM) glucose-treated cells (Figure 1F). These results show that alterations in glucose availability cause hyperpolarization of the mitochondrial inner membrane.

Alteration in media glucose levels regulates Pgp function and expression

Considering cellular ROS generation after glucose modulation (Figure 1B,D and E), and that ROS signalling alters cellular phenotype (Dworakowski *et al.*, 2006), we assessed if

glucose modulation could promote MDR. In these studies, we examined intrinsic and glucose-induced Pgp expression (Figure 2A, Bi), in addition to plasma membrane Pgp function, in KB31 (–Pgp) and KBV1 (+Pgp) cells (Figure 2Bii, Ci,ii). Furthermore, to assess if the response was cell type-specific, A549 and DMS-53 cells, which endogenously express Pgp, were also examined (Figure 2A,B and Ciii,iv).

All cell types were subjected to a shift in glucose levels during a 24 h/37°C incubation, after which protein levels were assessed by Western blotting utilizing an isolated membrane fraction. No Pgp was detected in KB31 cells under all conditions (Figure 2A). This finding was irrespective of the very high protein-loading and exposure time of KB31 cells (i.e., 500 μg and 300 s exposure time; Figure 2A). In contrast, modulation of glucose concentrations using KBV1, DMS-53 or A549 cells, resulted in significantly ($P < 0.05$) increased Pgp expression (Figure 2A). Notably, as evident from the lower protein loading and shorter exposure time (i.e., 30 μg and 40 s; Figure 2A), Pgp expression in KBV1 cells was far greater than in A549 or DMS-53 cells (i.e., protein load: 150 μg and exposure time: 120 s; Figure 2A).

To measure membrane Pgp levels, flow cytometry utilizing a FITC-labelled Pgp antibody was implemented (Figure 2Bi). This more sensitive method detected Pgp in all cell lines under normal glucose levels (25 mM). The Pgp levels were greatest in KBV1 cells followed by DMS-53, A549 and KB31 cells (Figure 2Bi). Notably, KB31 cells express only very low Pgp levels. Moreover, Pgp functionality in these cells under normal glucose (25 mM; Figure 2Bii) was found to correspond to total plasma membrane Pgp expression (Figure 2Bi), as measured by the accumulation of the fluorescent Pgp substrate, Rh123, in all cell types *via* flow cytometry (Figure 2Bii). In this case, low cellular Rh123 accumulation indicates high Pgp activity and efflux of Rh123 out of cells.

Interestingly, varying glucose to low (0 mM) or high (50 mM) concentrations for 24 h/37°C, only slightly, but significantly ($P < 0.05$), decreased Rh123 accumulation relative to normal glucose (25 mM) in KB31 cells (Figure 2Ci). The other three cell types that express significant Pgp levels (i.e., KBV1, A549 and DMS53; Figure 2A and Bi, showed a far more pronounced and significant ($P < 0.001$–0.05) decrease in Rh123 accumulation upon changing glucose concentrations from normal levels (25 mM; Figure 2Cii-iv). This latter observation is consistent with increased Pgp-mediated efflux of Rh123 under glucose-induced stress. Indeed, Rh123 accumulation was Pgp-dependent, as the potent Pgp inhibitor, Ela (0.2 μM) (Akhtar *et al.*, 2011), significantly ($P < 0.001$) increased Rh123 accumulation in KBV1, A549 and DMS-53 cells (Figure 2Cii-iv). The greater effect of Ela in KBV1, A549 and DMS-53 cells relative to KB31 cells, was probably due to their much higher Pgp levels (Figure 2A and Bi).

In these studies in Figure 2C, ROS were found to be important for increasing Pgp function, as incubation with NAC significantly ($P < 0.001$–0.05) reversed the glucose-induced increase in Pgp activity (at 0 and 50 mM glucose) relative to the respective glucose treatment only, as measured by Rh123 accumulation (Figure 2Ci-iv). This was particularly evident in cells expressing significant Pgp levels (i.e., KBV1, A549 and DMS53; Figure 2Cii-iv). Hence, these findings using NAC suggest ROS could be responsible for the increased Pgp expression at low and high glucose levels. Collectively, these observations in Figure 2 demonstrate that changes in glucose concentration lead to a higher Pgp-expressing phenotype. Therefore, to elucidate how glucose regulates Pgp expression, further mechanistic studies were performed utilizing KBV1 cells to take advantage of their marked Pgp expression/function.

Glucose variation-induced stress increases NF-κB nuclear translocation

During stress, HIF-1α is transcriptionally regulated by the redox-sensitive transcription factor, NF-κB, which binds at a distinct element in the promoter of the *HIF-1α* gene (van Uden *et al.*, 2008). Therefore, we investigated the impact of glucose levels on NF-κB activity. Considering that NF-κB transcriptional activity requires translocation of its p65 subunit from the cytosol to the nucleus (Ghosh and Hayden, 2008), we initially investigated p65 expression in nuclear and cytosolic extracts of KBV1 (+Pgp) cells by Western blotting (Figure 3A). Expression of HDAC1 and GAPDH were only expressed in the nuclear and cytosolic fractions respectively.

Incubating cells for 4 h/37°C with low (0 or 12.5 mM) or high (50 mM) glucose levels or with H_2O_2 (50 μM) did not significantly ($P > 0.05$) increase total p65 expression in KBV1 whole cell lysates relative to normal (25 mM) glucose-treated cells (Figure 3Ai). However, varying glucose concentrations (0, 12.5 and 50.0 mM) relative to normal levels (25 mM), significantly ($P < 0.001$–0.05) decreased p65 expression in the cytosol relative to normal (25 mM) glucose (Figure 3Aii).

In contrast to the cytosolic fraction, a significant ($P < 0.001$) increase in p65 was detected in the nuclear fraction at low (0 mM) and high (50 mM) glucose treatments relative to the normal (25 mM) glucose-treated cells (Figure 3Aiii). Hence, the studies in Figure 3A demonstrate that following low (0 mM) or high (50 mM) glucose treatments, marked p65 translocation from the cytosol to nucleus occurred.

The effect of glucose treatments on nuclear p65 was also assessed by immunofluorescence microscopy (Figure 3B). Relative to normal glucose (25 mM), incubation of KBV1 cells with low glucose (0, 12.5 mM) or high glucose (50 mM) led to nuclear p65 accumulation, as demonstrated by merging p65 (red) with DAPI (blue), forming a purple co-localization pattern (Figure 3Bi; see boxes as relevant examples of purple co-localization in the merged image). Quantification of p65 nuclear intensity demonstrated that H_2O_2 or low and high glucose relative to normal glucose levels, significantly ($P < 0.001$) increased p65 nuclear localization in KBV1 cells (Figure 3Bii). These findings demonstrate variations in glucose caused nuclear translocation of the NF-κB p65 subunit.

Glucose variation-induced stress regulates HIF-1α and MDR1 expression in MDR tumour cells

Importantly, it is known that HIF-1α is up-regulated by NF-κB (van Uden *et al.*, 2008) and can increase Pgp expression (Comerford *et al.*, 2002). Considering this, we examined the molecular events following glucose variation-induced stress in KBV1 (+Pgp) cells by examining the mRNA expression of *HIF-1α*, and its target gene, *MDR1* (encoding Pgp). The glucose transporter gene, *GLUT1*, was used as a control as it

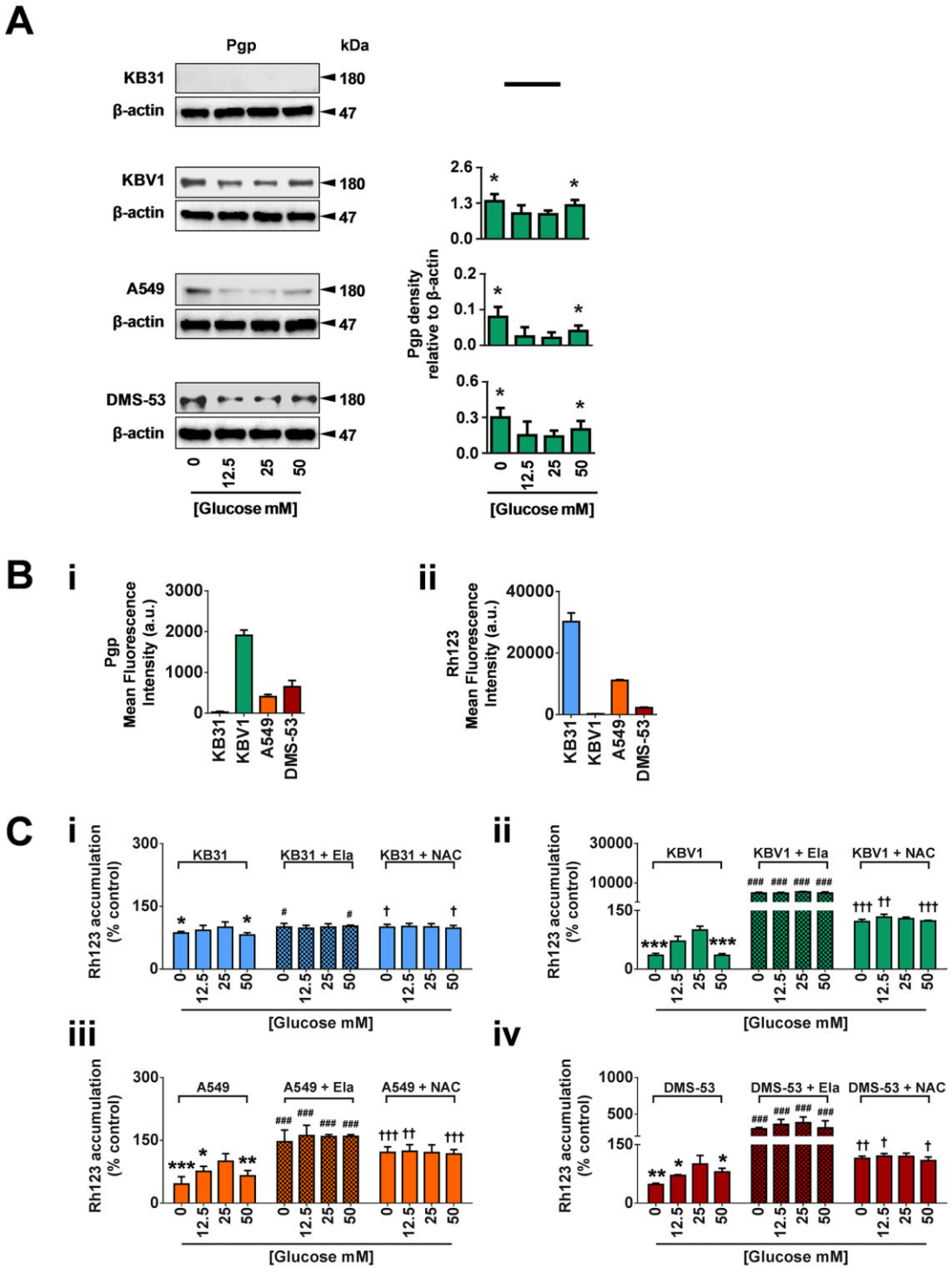

Figure 2

Changes in glucose levels increase Pgp-expression and function. KB31, KBV1, A549 and DMS-53 cells were examined for: (A) Pgp protein expression assessed by Western blotting following a change from the normal glucose level (25 mM) to low (0 or 12.5 mM) or high (50 mM) glucose after a 24 h/37°C incubation; (B)(i) Cell plasma membrane Pgp measured by flow cytometry under conditions of normal glucose (25 mM); (ii) Pgp function analysis by flow cytometric measurement of the intracellular accumulation of Rh123 in normal glucose (25 mM) over a 30 min/37°C incubation. (C) Decreased intracellular Rh123-accumulation following a 24 h/37°C incubation with low or high glucose. The Pgp inhibitor, Ela (0.2 μM), or antioxidant NAC (5 mM), increased cellular accumulation of Rh123 in all treatment conditions relative to its respective glucose treatment alone in KBV1, A549 and DMS-53 cells. The results in (A) are typical of three experiments, densitometry is mean ± SD ($n = 3$). *$P < 0.05$, relative to normal glucose (25 mM). For (B), mean fluorescence intensity is presented as arbitrary units (a.u.). Results in (C) are mean ± SD ($n = 5$). *$P < 0.05$, **$P < 0.01$, ***$P < 0.001$, versus normal glucose (25 mM), $^{\#}P < 0.05$, $^{\#\#\#}P < 0.001$, $^{\dagger}P < 0.05$, $^{\dagger\dagger}P < 0.01$, $^{\dagger\dagger\dagger}P < 0.001$ versus respective glucose treatment alone.

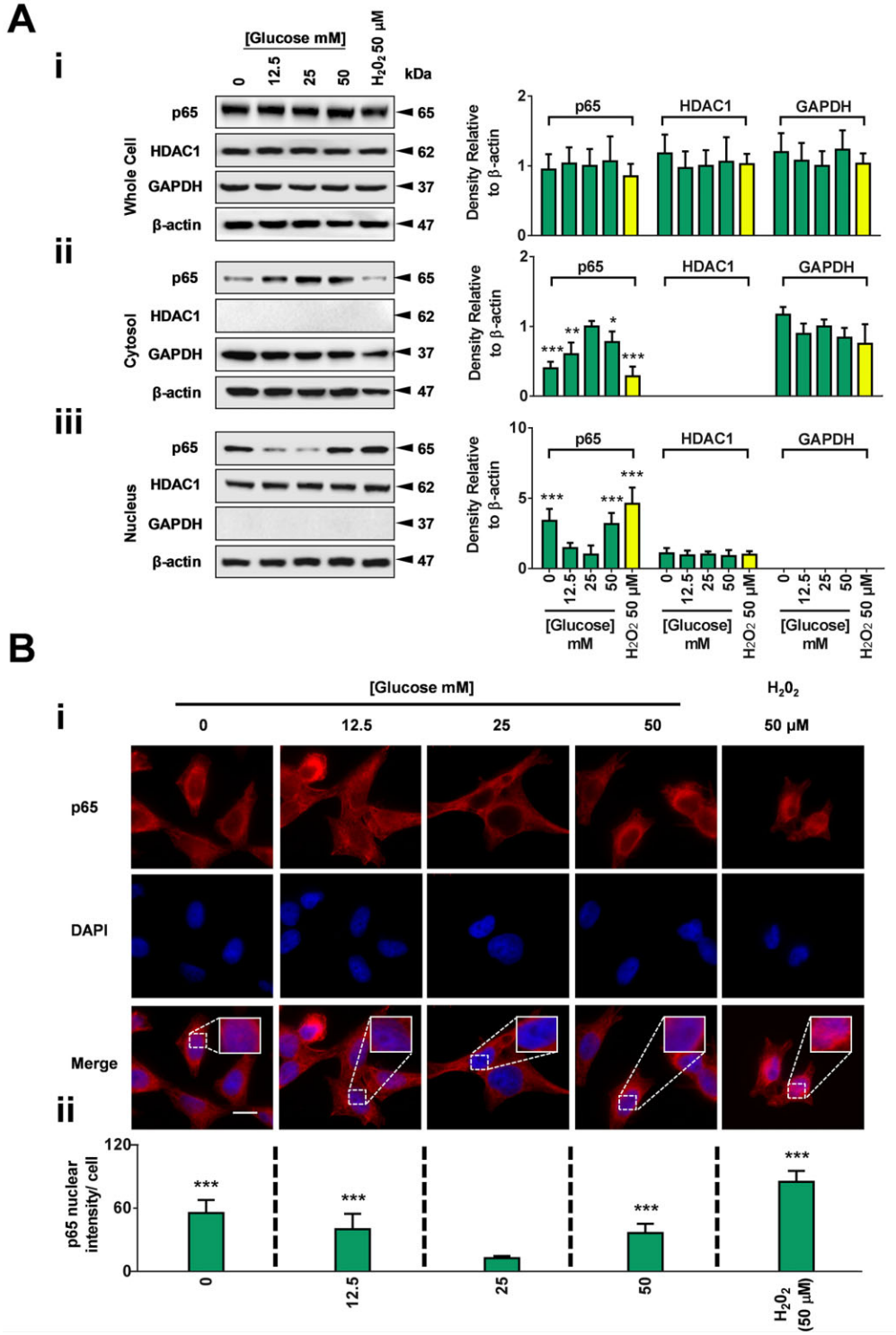

Figure 3

Changes in glucose levels induce translocation of the activated NF-κB p65 subunit into the nucleus. Analysis of KBV1 cells for (A) p65 expression in: (i) whole cells; (ii) the cytosolic fraction; and (iii) nuclear fraction, demonstrates a decrease in cytosolic p65 protein levels with a simultaneous increase in nuclear p65 protein accumulation after a 24 h/37°C incubation with low (0 and 12.5 mM) or high (50 mM) glucose. Fraction purity was confirmed with HDAC1 (nuclear marker) and GAPDH (cytosolic marker). (B) Immunofluorescence detection of p65 co-localization with the nuclear marker, DAPI, in KBV1 cells following a 4 h/37°C incubation with low, normal and high glucose levels. Co-localization of p65 with the nuclear marker, DAPI, was quantified as fluorescence intensity per cell. The results in (Ai–iii) are typical of three experiments, while densitometry is mean ± SD (n = 3). *P < 0.05, **P < 0.01, ***P < 0.001 relative to normal glucose (25 mM). Immunofluorescence photographs in (Bi) are representative of three experiments and the quantified fluorescence intensity in (Bii) is mean ± SD (n = 3). Scale bar: 10 μm in each panel.

displays a well-characterized homeostatic response to glucose, with low cellular glucose levels up-regulating its mRNA and high cellular glucose leading to its down-regulation (Mandarino *et al.*, 1994; Hayashi *et al.*, 2004; Thorens and Mueckler, 2010). In these studies, there was significant ($P < 0.001$–0.01) up-regulation of *HIF-1α*- and *MDR1*-mRNA expression following the low glucose (0 mM) and high glucose (50 mM) treatments for 24 h compared with normal glucose levels (25 mM; Figure 4A). *GLUT1*-mRNA significantly ($P < 0.001$) increased with glucose starvation (0 mM) relative to normal glucose (25 mM), but significantly ($P < 0.05$) decreased relative to the normal control (25 mM) at high (50 mM) glucose levels (Figure 4A). The positive control, H_2O_2, significantly ($P < 0.001$) up-regulated *HIF-1α*-, *MDR1*- and *GLUT1*-mRNA expression (Figure 4A). Hence, *HIF-1α*- and *MDR1*-mRNA demonstrate similar responses to glucose modulation and H_2O_2-mediated redox stress.

Glucose variation-induced stress regulates HIF-1α- and Pgp protein expression in MDR tumour cells

The translation of *HIF-1α*- and *MDR1*-mRNA was confirmed, as their protein levels were significantly ($P < 0.01$) increased in KBV1 cells following low (0 mM) and high (50 mM) glucose treatments for 24 h relative to normal glucose levels (25 mM; Figure 4B). Notably, HIF-1α appeared as two closely associated bands (Figure 4B), which are due to post-transcriptional modification (Zagzag *et al.*, 2005). In contrast, GLUT1 protein remained inversely proportional to glucose availability (Figure 4B), as reported (Mandarino *et al.*, 1994; Hayashi *et al.*, 2004). The positive controls, H_2O_2 and AM, significantly ($P < 0.01$) increased HIF1α- and Pgp expression relative to normal glucose (25 mM), while it significantly ($P < 0.01$) decreased GLUT1 relative to normal glucose (25 mM; Figure 4B).

Considering the results mentioned earlier, PHD2 protein expression was then examined as it is responsible for oxygen-dependent degradation of HIF-1α (Bruick and McKnight, 2001), and may be regulated by altered glucose. Under the glucose levels used, PHD2 expression was inversely correlated to HIF-1α- and Pgp levels (Figure 4B). In fact, at lower (0 and 12.5 mM) and higher (50 mM) glucose, PHD2 expression was significantly ($P < 0.01$–0.05) decreased relative to normal (25 mM) glucose. The antioxidant, NAC (De Flora *et al.*, 1995), and the NOX inhibitor, apocynin (Petronio *et al.*, 2013), prevented the glucose variation-induced regulation of HIF-1α, Pgp, GLUT1 and PHD2 expression (Figure 4B).

Hence, at the lowest and highest glucose concentrations, greater HIF-1α expression was observed, which corresponded to the increased nuclear p65 (Figure 3Aiii and Bi,ii) and decreased HIF-1α degradation by PHD2 at these glucose levels relative to normal glucose (Figure 4B). This process can be prevented by an antioxidant or the inhibition of NOX.

Alterations in glucose increases HIF-1 promoter binding activity

To monitor HIF-1-regulated signal transduction pathways during glucose modulation, KBV1 cells were transfected with a *HIF-1* promoter luciferase construct. Cells were also transfected with a constitutively expressing *Renilla* luciferase construct and a non-inducible Firefly luciferase construct which acted as positive and negative controls, respectively, to validate transfection (see 'Positive' and 'Negative'; Figure 4C). The *HIF-1* promoter-binding activity (see 'Test'; Figure 4C) significantly ($P < 0.001$–0.01) increased following incubation of cells for 24 h with low (0 and 12.5 mM) or high (50 mM) glucose compared with normal glucose (25 mM; Figure 4C). This increase in *HIF-1* promoter-binding activity was consistent with elevated HIF-1α protein levels at low and high glucose (Figure 4B) *via* p65 transcription factor translocation (Figure 3Aiii and Bi,ii).

Alterations in glucose modulates Pgp-induced DOX resistance

Considering that altering glucose levels changed Pgp transport activity (Figure 2C), we next examined if glucose modulation also results in Pgp-induced resistance to the chemotherapeutic agent and Pgp substrate, DOX (Shen *et al.*, 2008) (Figure 5). Initial studies examined KB31 cells which express the lowest Pgp levels among the cell types (Figure 2A and Bi), and displayed slight, but detectable alterations in Pgp transport activity upon modulating glucose (Figure 2Ci). A 72 h incubation of KB31 cells with low (0 mM) or high glucose (50 mM), compared with normal (25 mM) glucose levels significantly ($P < 0.01$) increased the DOX IC_{50} (i.e., concentration required for 50% inhibition of cellular proliferation; Figure 5A). This observation indicated that glucose variation increases DOX resistance, as higher DOX concentrations were required to inhibit proliferation (i.e., higher IC_{50}; Figure 5A). Hence, these results demonstrate that incubation of KB31 cells under glucose starvation conditions, results in increased Pgp activity, which leads to enhanced resistance to DOX and a higher IC_{50} value. The role of Pgp in this increased resistance was confirmed by the Pgp inhibitor, Ela, which significantly ($P < 0.01$–0.05) reversed the IC_{50} to levels similar to normal glucose (25 mM).

Similarly, in KBV1 cells that possess the highest Pgp expression and activity following low (0 mM) and high (50 mM) glucose treatment (Figure 2), there was a far more marked and significant ($P < 0.001$) increase in the DOX IC_{50} value compared with normal glucose (25 mM; Figure 5B) relative to KB31 cells (Figure 5A). Moreover, the effect of Pgp inhibition with Ela was significant ($P < 0.001$) for all glucose levels, reducing the DOX IC_{50} to similar levels as non-Pgp-expressing KB31 cells (Figure 5A and B). Notably, Ela also reversed resistance of KBV1 cells to DOX observed at normal glucose levels (25 mM; Figure 5B), as this cell type expresses high Pgp levels and activity under these conditions (Figure 2A, Bi and Bii). The A549 and DMS-53 cell types, which express appreciable Pgp (Figure 2A and Bi), showed similar results as KBV1 cells (Figure 5C and D).

Collectively, these data indicate that glucose levels regulate the sensitivity of cancer cells to DOX *via* Pgp induction. This effect was most pronounced in KBV1 cells that highly express Pgp, but could also be detected in KB31 cells that express much lower Pgp levels.

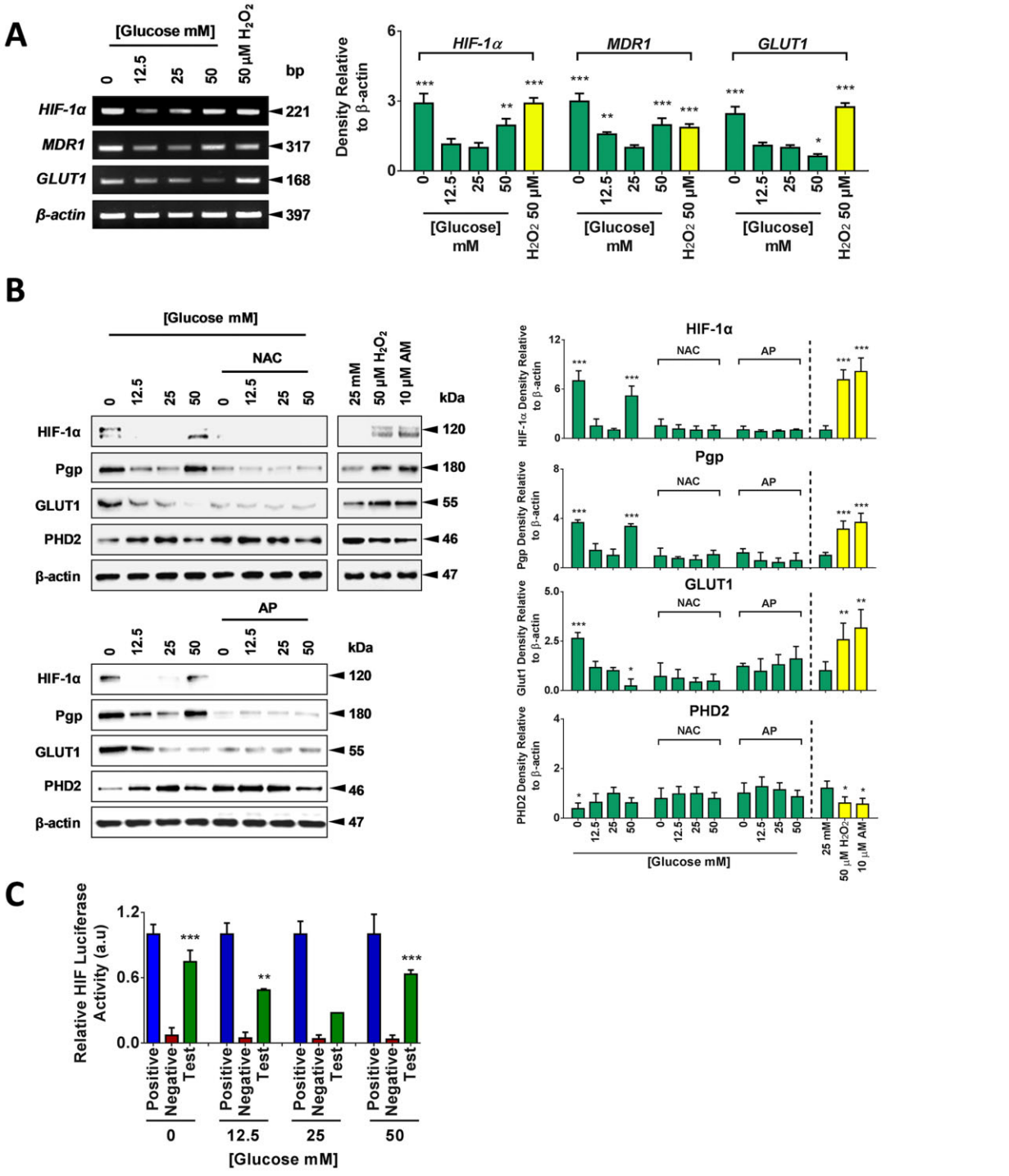

Figure 4

Changes in glucose levels regulate the mRNA and protein levels of HIF-1α, *MDR1* (Pgp) and GLUT1, and the protein levels of PHD2. Analysis of KBV1 cells show: (A) increased *HIF-1α*- and Pgp- (*MDR1*) mRNA expression *via* RT-PCR after a 24 h/37°C incubation with low (0 mM), normal (25 mM), or high (50 mM) glucose levels. *GLUT1* mRNA expression was inversely proportional to glucose levels. (B) Increased Pgp and HIF-1α protein expression measured by Western blot after a 24 h/37°C incubation with low (0 and 12.5 mM), normal (25 mM) and high (50 mM) glucose. GLUT1 protein levels were inversely proportional to glucose levels. PHD2-protein expression was decreased after varying glucose levels from normal glucose (25 mM). The antioxidant, NAC (5 mM) or the NOX inhibitor, apocynin (50 μM) prevented the glucose variation-induced regulation of HIF-1α, Pgp, GLUT1 and PHD2 expression. H_2O_2 and AM (10 μM) were used as positive controls for the effects of ROS. (C) *HIF-1α* promoter-binding activity under varying glucose levels (see 'Test'). The results in (A, B) are typical of three experiments with the densitometry being mean ± SD ($n = 3$). *$P < 0.05$, **$P < 0.01$, ***$P < 0.001$ relative to normal glucose (25 mM). The results in (C) are presented as arbitrary units (a.u.) and are mean ± SD ($n = 3$). **$P < 0.01$, ***$P < 0.001$, relative to the respective control (i.e., normal glucose at 25 mM).

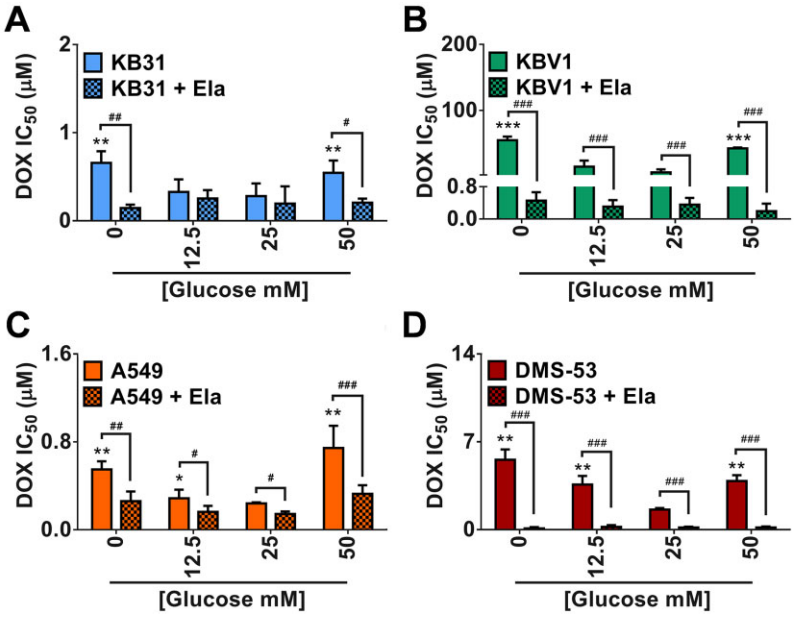

Figure 5

Glucose-induced stress increases cellular resistance to the chemotherapeutic and Pgp-substrate, DOX. Cellular proliferation of: (A) KB31, (B) KBV1, (C) A549 and (D) DMS-53 cells in culture using medium supplemented with low (0 and 12.5 mM), normal (25 mM), or high glucose (50 mM) concentrations for 24 h/37°C before and during the incubation with DOX (24 h/37°C). Studies were performed in the presence or absence of the Pgp inhibitor Ela (0.2 μM). Results in (A–D) are mean ± SD ($n = 4$). $^{*}P < 0.05$, $^{**}P < 0.01$, $^{***}P < 0.001$, versus normal glucose (25 mM), $^{\#}P < 0.05$, $^{\#\#}P < 0.01$, $^{\#\#\#}P < 0.001$ versus respective glucose treatment concentration.

Discussion

Tumour cells exist in a stressful micro-environment, where crucial nutrients, such as glucose and oxygen, are heterogeneous (Pelicano *et al.*, 2006; Annibaldi and Widmann, 2010). As a consequence, cancer cells are constantly adapting their metabolism to the tumour micro-environment. This investigation assessed how glucose variation-induced stress affected drug resistance in a cell culture model. To achieve this, glucose levels were altered to either a lower or higher glucose level to induce stress. Collectively, the present studies show that cancer cells develop a resistant phenotype upon ROS generation because of altered glucose availability.

The generation of ROS plays an important role in regulating genes responsible for the metabolic differences between normal and cancer cells (Denko, 2008; Hagen, 2012). Interestingly, ROS have been demonstrated to regulate downstream target genes of NF-κB and HIF-1α, including vascular endothelial growth factor A (VEGFA; Liu *et al.*, 2006), which promotes angiogenesis (Byrne *et al.*, 2005; Pages and Pouyssegur, 2005) and GLUT1, which activates glucose transport (Hayashi *et al.*, 2004; Thorens and Mueckler, 2010). These intracellular ROS are primarily generated *via* NOX and are also formed as a by-product of the electron transport chain (Murphy, 2009; Block and Gorin, 2012). This study demonstrates that altered glucose levels increase ROS (Figure 1B, D and E) and that decreasing NOX activity or NOX4 protein levels reduces oxidative species generation following glucose modulation (Figure 1D). Additionally, the superoxide indicator, MitoSOX, demonstrated some mitochondrial superoxide generation as a consequence of altered glucose levels (Figure 1E), with the mitochondrial membrane becoming hyper-polarized (Figure 1F). Indeed, inhibition of NOX has been shown to inhibit glucose withdrawal-induced ROS (Graham *et al.*, 2012). Also, mitochondrial ROS are linked to mitochondrial membrane potential (Griffiths, 2000), with hyperpolarization promoting ROS production through mitochondrial complex I (Yu *et al.*, 2006). Together, ROS primarily from NOX4, and to a lesser extent, the mitochondrial complex, explain glucose variation-induced ROS generation (Figure 1B and 6).

While ROS can mediate cytotoxicity, there is also evidence to support their role in signal transduction (Behrend *et al.*, 2003). In the current investigation, we observed that alterations in glucose levels resulted in increased Pgp expression (Figure 2A) and function (Figure 2Ci-iv), which was more apparent in cells with higher basal Pgp. As a consequence of glucose modulation, the involvement of ROS-mediated signalling (Behrend *et al.*, 2003), was substantiated by significantly reduced Pgp activity *via* the antioxidant, NAC (Figure 2C). In agreement with our studies, up-regulation of Pgp expression was found when the antioxidant, glutathione, was depleted in rat brain endothelial cells (Hong *et al.*, 2006).

Although previous studies showed that glucose deprivation abolishes Pgp activity through ATP restriction (Sauna and Ambudkar, 2007), we demonstrated that Pgp activity remains increased under such conditions, as measured by decreased Rh123 accumulation and increased Pgp expression (Figure 2B and C). Interestingly, it has been shown that while complete glucose starvation reduces ATP levels to 50%, this is not sufficient to reduce Pgp activity (Trach *et al.*, 2012). This may be a result of the cell utilizing alternative metabolic

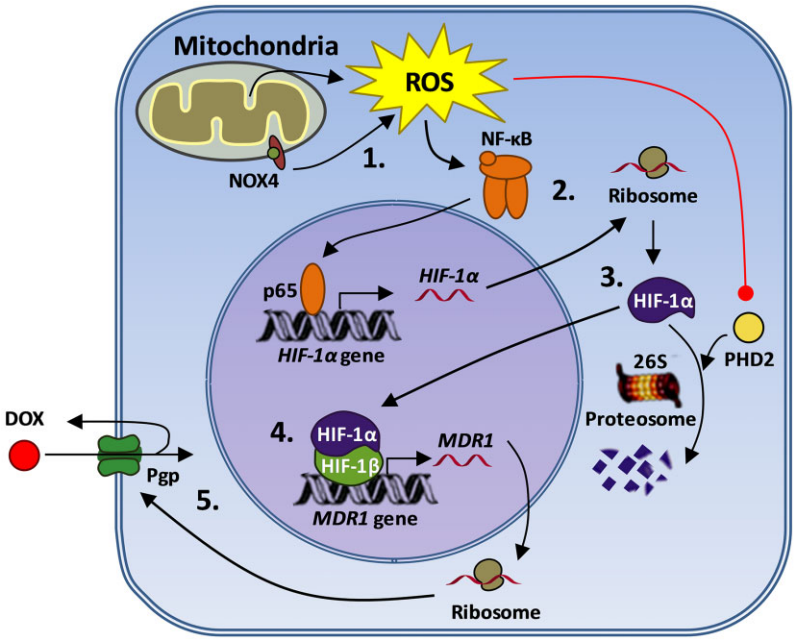

Figure 6

Schematic illustration of the glucose-induced Pgp resistance phenotype observed in this study. Alterations in glucose concentrations induces: (i) production of mitochondrial ROS *via* primarily the NOX4 enzyme, but also the electron-transport chain; (ii) translocation of NF-κB's active p65 subunit into the nucleus, where it is able to induce transcription of the master transcription factor; HIF-1α; (iii) decreased expression of PHD2, which prevents degradation of HIF-1α *via* the proteosome; (iv) increased expression of HIF-1, that binds to the hypoxia-response element (HRE) in the *MDR1* gene promoter and leads to transcription of *Pgp* mRNA (*MDR1*) and its subsequent translation; and (v) increased Pgp on the plasma membrane, which acts as a 'drug-pump' to increase efflux of the cytotoxic Pgp substrate, DOX, from the cell. This response induces resistance to this chemotherapeutic.

sources for ATP production, such as fatty acids and proteins (Hsu and Sabatini, 2008). This may explain the sustained Pgp activity in our studies during glucose starvation.

The oxidant-inducible transcription factor, NF-κB (Piva *et al.*, 2006), requires translocation of its p65 subunit to the nucleus (Oeckinghaus and Ghosh, 2009) to modulate HIF-1α expression during oxidative stress (Belaiba *et al.*, 2007). In this investigation, glucose-induced stress led to translocation of the p65 subunit of NF-κB to the nucleus (Figure 3Aiii and Bi,ii). Consistent with p65 nuclear localization, increased HIF-1α expression was observed following alterations in glucose levels (Figure 4A and B), with a *HIF*-reporter assay confirming activation of HIF-regulated signal transduction (Figure 4C). Further, upon glucose-induced stress, reduced PHD2 expression also occurred (Figure 4B), which will decrease HIF-1α degradation (Bruick and McKnight, 2001). Hence, under these conditions, increased HIF-1α can induce Pgp transcription (Marxsen *et al.*, 2004). Importantly, the central role of ROS in this pathway was confirmed by the utilization of the antioxidant, NAC or the NOX inhibitor, apocynin, which suppressed glucose-induced HIF-1α induction, while preventing the decrease in PHD2 (Figure 4B). This inhibition of ROS generation also resulted in decreased Pgp expression, indicating that glucose-induced ROS production was responsible for the observed increase in Pgp expression (Figure 6).

The present studies also demonstrated that cancer cells develop a resistant phenotype to the chemotherapeutic substrate, DOX, upon altered glucose availability. The increase in glucose-induced resistance was found to be due to Pgp, as co-incubation with the Pgp inhibitor, Ela, reversed DOX resistance (Figure 5). While the focus of this paper was Pgp, glucose variation-induced ROS may also regulate the expression of other ABC transporters including ABCG2 and MRP1, which are also HIF-1 responsive (Chen *et al.*, 2009; Mo and Zhang, 2012). However, unlike the Pgp inhibitor, Ela, studies using the ABCG2 inhibitor, KO143 (Allen *et al.*, 2002), or the MRP1 inhibitor, MK571 (van der Kolk *et al.*, 1998), did not alter the cytotoxicity of DOX in the KBV1 cells which hyper-expressed Pgp in our studies (data not shown). This observation suggests that the glucose-induced resistance observed was due to Pgp expression.

Hence, our findings highlight that MDR might not only arise from repeated treatment of patients with anti-cancer drugs that can select for cells with high Pgp expression, but can also occur as a consequence of the stressful tumour micro-environment. As such, enhanced MDR because of glucose-induced stress could play a vital role in the response of tumours to chemotherapeutics.

Conclusions

Herein, for the first time, we show that glucose-induced stress acts to increase HIF-1α activity, resulting in increased Pgp expression and function in a culture model. Consequently, the resulting MDR phenotype increased DOX

resistance. These studies highlight the potential importance of the tumour micro-environment in MDR and are important to consider for cancer treatment and future drug development.

Acknowledgements

N. A. S. thanks the University of Sydney for an Australian Postgraduate Award. D. R. R. appreciates support from the National Health and Medical Research Council of Australia for a Senior Principal Research Fellowship and Project Grant funding. P. J. J. kindly acknowledges the Cancer Institute New South Wales (CINSW) for an Early Career Research Fellowship.

Author contributions

P. J. J. and D. R. R. contributed equally to the work as co-corresponding and senior authors; P. J. J., N. A. S. and D. R. R. planned the research; P. J .J. and D. R. R.-directed experiments; N. A. S. performed experiments; all of the authors analysed data; N. A. S, D. R. R. and P. J. J. wrote the paper.

Conflicts of interest

None.

References

Akhtar N, Ahad A, Khar RK, Jaggi M, Aqil M, Iqbal Z *et al*. (2011). The emerging role of P-glycoprotein inhibitors in drug delivery: a patent review. Expert Opin Ther Pat 21: 561–576.

Alexander SPH, Benson HE, Faccenda E, Pawson AJ, Sharman JL, Spedding M *et al*. (2013a). The Concise Guide to PHARMACOLOGY 2013/14: Transporters. Br J Pharmacol. 170: 1706–1796.

Alexander SPH, Benson HE, Faccenda E, Pawson AJ, Sharman JL, Spedding M *et al*. (2013b). The Concise Guide to PHARMACOLOGY 2013/14: Enzymes. Br J Pharmacol. 170: 1797–1867.

Allen JD, van Loevezijn A, Lakhai JM, van der Valk M, van Tellingen O, Reid G *et al*. (2002). Potent and specific inhibition of the breast cancer resistance protein multidrug transporter in vitro and in mouse intestine by a novel analogue of fumitremorgin C. Mol Cancer Ther 1: 417–425.

Annibaldi A, Widmann C (2010). Glucose metabolism in cancer cells. Curr Opin Clin Nutr Metab Care 13: 466–470.

Behrend L, Henderson G, Zwacka RM (2003). Reactive oxygen species in oncogenic transformation. Biochem Soc Trans 31: 1441–1444.

Belaiba RS, Bonello S, Zahringer C, Schmidt S, Hess J, Kietzmann T *et al*. (2007). Hypoxia up-regulates hypoxia-inducible factor-1alpha transcription by involving phosphatidylinositol 3-kinase and nuclear factor kappaB in pulmonary artery smooth muscle cells. Mol Biol Cell 18: 4691–4697.

Block K, Gorin Y (2012). Aiding and abetting roles of NOX oxidases in cellular transformation. Nat Rev Cancer 12: 627–637.

Bruick RK, McKnight SL (2001). A conserved family of prolyl-4-hydroxylases that modify HIF. Science 294: 1337–1340.

Byrne AM, Bouchier-Hayes DJ, Harmey JH (2005). Angiogenic and cell survival functions of vascular endothelial growth factor (VEGF). J Cell Mol Med 9: 777–794.

Casciari JJ, Sotirchos SV, Sutherland RM (1988). Glucose diffusivity in multicellular tumor spheroids. Cancer Res 48: 3905–3909.

Chaoui D, Faussat AM, Majdak P, Tang R, Perrot JY, Pasco S *et al*. (2006). JC-1, a sensitive probe for a simultaneous detection of P-glycoprotein activity and apoptosis in leukemic cells. Cytometry B Clin Cytom 70: 189–196.

Chaplain MAJ (1996). Avascular growth, angiogenesis and vascular growth in solid tumours: the mathematical modelling of the stages of tumour development. Math Comput Model 23: 47–87.

Chen J-Q, Russo J (2012). Dysregulation of glucose transport, glycolysis, TCA cycle and glutaminolysis by oncogenes and tumor suppressors in cancer cells. Biochim Biophys Acta 1826: 370–384.

Chen L, Feng P, Li S, Long D, Cheng J, Lu Y *et al*. (2009). Effect of hypoxia-inducible factor-1alpha silencing on the sensitivity of human brain glioma cells to doxorubicin and etoposide. Neurochem Res 34: 984–990.

Comerford KM, Wallace TJ, Karhausen J, Louis NA, Montalto MC, Colgan SP (2002). Hypoxia-inducible factor-1-dependent regulation of the multidrug resistance (MDR1) gene. Cancer Res 62: 3387–3394.

De Flora S, Cesarone CF, Balansky RM, Albini A, D'Agostini F, Bennicelli C *et al*. (1995). Chemopreventive properties and mechanisms of *N*-acetylcysteine. The experimental background. J Cell Biochem Suppl 22: 33–41.

Denko NC (2008). Hypoxia, HIF1 and glucose metabolism in the solid tumour. Nat Rev Cancer 8: 705–713.

Dworakowski R, Anilkumar N, Zhang M, Shah AM (2006). Redox signalling involving NADPH oxidase-derived reactive oxygen species. Biochem Soc Trans 34 (Pt 5): 960–964.

Ghosh S, Hayden MS (2008). New regulators of NF-kappaB in inflammation. Nat Rev Immunol 8: 837–848.

Graham NA, Tahmasian M, Kohli B, Komisopoulou E, Zhu M, Vivanco I *et al*. (2012). Glucose deprivation activates a metabolic and signaling amplification loop leading to cell death. Mol Syst Biol 8: 589–605.

Griffiths EJ (2000). Mitochondria – potential role in cell life and death. Cardiovasc Res 46: 24–27.

Hagen T (2012). Oxygen versus reactive oxygen in the regulation of HIF-1: the balance tips. Biochem Res Int 2012: 436981. doi:10.1155/2012/436981

Hayashi M, Sakata M, Takeda T, Yamamoto T, Okamoto Y, Sawada K *et al*. (2004). Induction of glucose transporter 1 expression through hypoxia-inducible factor 1alpha under hypoxic conditions in trophoblast-derived cells. J Endocrinol 183: 145–154.

Hong H, Lu Y, Ji ZN, Liu GQ (2006). Up-regulation of P-glycoprotein expression by glutathione depletion-induced oxidative stress in rat brain microvessel endothelial cells. J Neurochem 98: 1465–1473.

Hsu PP, Sabatini DM (2008). Cancer cell metabolism: warburg and beyond. Cell 134: 703–707.

Jansson PJ, Sharpe PC, Bernhardt PV, Richardson DR (2010). Novel thiosemicarbazones of the ApT and DpT series and their copper complexes: identification of pronounced redox activity and characterization of their antitumor activity. J Med Chem 53: 5759–5769.

Karlsson M, Kurz T, Brunk UT, Nilsson SE, Frennesson CI (2010). What does the commonly used DCF test for oxidative stress really show? Biochem J 428: 183–190.

Kawabata M, Kobayashi H, Mori S, Sekiguchi S, Takemura Y (1997). Flow cytometric analysis of P-glycoprotein function by rhodamine 123 dye-efflux assay in human leukemia cells]. Rinsho Byori 45: 891–898.

Keston AS, Brandt R (1965). The fluorometric analysis of ultramicro quantities of hydrogen peroxide. Anal Biochem 11: 1–5.

van der Kolk DM, de Vries EG, Koning JA, van den Berg E, Muller M, Vellenga E (1998). Activity and expression of the multidrug resistance proteins MRP1 and MRP2 in acute myeloid leukemia cells, tumor cell lines, and normal hematopoietic CD34+ peripheral blood cells. Clin Cancer Res 4: 1727–1736.

Kovacevic Z, Chikhani S, Lui GY, Sivagurunathan S, Richardson DR (2013). The iron-regulated metastasis suppressor NDRG1 targets NEDD4L, PTEN, and SMAD4 and inhibits the PI3K and Ras signaling pathways. Antioxid Redox Signal 18: 874–887.

Li J, Zhu H, Shen E, Wan L, Arnold JM, Peng T (2010). Deficiency of rac1 blocks NADPH oxidase activation, inhibits endoplasmic reticulum stress, and reduces myocardial remodeling in a mouse model of type 1 diabetes. Diabetes 59: 2033–2042.

Liu LZ, Hu XW, Xia C, He J, Zhou Q, Shi X *et al.* (2006). Reactive oxygen species regulate epidermal growth factor-induced vascular endothelial growth factor and hypoxia-inducible factor-1alpha expression through activation of AKT and P70S6K1 in human ovarian cancer cells. Free Radic Biol Med 41: 1521–1533.

Longley DB, Johnston PG (2005). Molecular mechanisms of drug resistance. J Pathol 205: 275–292.

Ludwig JA, Szakacs G, Martin SE, Chu BF, Cardarelli C, Sauna ZE *et al.* (2006). Selective toxicity of NSC73306 in MDR1-positive cells as a new strategy to circumvent multidrug resistance in cancer. Cancer Res 66: 4808–4815.

Mandarino LJ, Finlayson J, Hassell JR (1994). High glucose downregulates glucose transport activity in retinal capillary pericytes but not endothelial cells. Invest Ophthalmol Vis Sci 35: 964–972.

Marxsen JH, Stengel P, Doege K, Heikkinen P, Jokilehto T, Wagner T *et al.* (2004). Hypoxia-inducible factor-1 (HIF-1) promotes its degradation by induction of HIF-alpha-prolyl-4-hydroxylases. Biochem J 381 (Pt 3): 761–767.

Mattiazzi M, Vijayvergiya C, Gajewski CD, DeVivo DC, Lenaz G, Wiedmann M *et al.* (2004). The mtDNA T8993G (NARP) mutation results in an impairment of oxidative phosphorylation that can be improved by antioxidants. Hum Mol Genet 13: 869–879.

Milane L, Duan ZF, Amiji M (2011). Role of hypoxia and glycolysis in the development of multi-drug resistance in human tumor cells and the establishment of an orthotopic multi-drug resistant tumor model in nude mice using hypoxic pre-conditioning. Cancer Cell Int 125: 5168–5176.

Mo W, Zhang JT (2012). Human ABCG2: structure, function, and its role in multidrug resistance. Int J Biochem Mol Biol 3: 1–27.

Mukhopadhyay P, Rajesh M, Yoshihiro K, Hasko G, Pacher P (2007). Simple quantitative detection of mitochondrial superoxide production in live cells. Biochem Biophys Res Commun 358: 203–208.

Murphy MP (2009). How mitochondria produce reactive oxygen species. Biochem J 417: 1–13.

Nickel A, Kohlhaas M, Maack C (2014). Mitochondrial reactive oxygen species production and elimination. J Mol Cell Cardiol 73: 26–33.

Oeckinghaus A, Ghosh S (2009). The NF-kappaB family of transcription factors and its regulation. Cold Spring Harb Perspect Biol 1: a000034.

Pages G, Pouyssegur J (2005). Transcriptional regulation of the vascular endothelial growth factor gene – a concert of activating factors. Cardiovasc Res 65: 564–573.

Pawson AJ, Sharman JL, Benson HE, Faccenda E, Alexander SP, Buneman OP *et al.*; NC-IUPHAR (2014). The IUPHAR/BPS Guide to PHARMACOLOGY: an expert-driven knowledgebase of drug targets and their ligands. Nucl. Acids Res. 42 (Database Issue): D1098–106.

Pelicano H, Martin DS, Xu RH, Huang P (2006). Glycolysis inhibition for anticancer treatment. Oncogene 25: 4633–4646.

Perelman A, Wachtel C, Cohen M, Haupt S, Shapiro H, Tzur A (2012). JC-1: alternative excitation wavelengths facilitate mitochondrial membrane potential cytometry. Cell Death Dis 3: e430.

Petronio MS, Zeraik ML, Fonseca LM, Ximenes VF (2013). Apocynin: chemical and biophysical properties of a NADPH oxidase inhibitor. Molecules 18: 2821–2839.

Piva R, Belardo G, Santoro MG (2006). NF-kappaB: a stress-regulated switch for cell survival. Antioxid Redox Signal 8: 478–486.

Prochazkova J, Kubala L, Kotasova H, Gudernova I, Sramkova Z, Pekarova M *et al.* (2011). ABC transporters affect the detection of intracellular oxidants by fluorescent probes. Free Radic Res 45: 779–787.

Richardson D, Tran E, Ponka P (1995). The potential of iron chelators of the pyridoxal isonicotinoyl hydrazone class as effective antiproliferative agents. Blood 86: 4295–4306.

Saletta F, Suryo Rahmanto Y, Richardson DR (2010). The translational regulator eIF3a: the tricky eIF3 subunit! Biochim Biophys Acta 1806: 275–286.

Sauna ZE, Ambudkar SV (2007). About a switch: how P-glycoprotein (ABCB1) harnesses the energy of ATP binding and hydrolysis to do mechanical work. Mol Cancer Ther 6: 13–23.

Shen F, Chu S, Bence AK, Bailey B, Xue X, Erickson PA *et al.* (2008). Quantitation of doxorubicin uptake, efflux, and modulation of multidrug resistance (MDR) in MDR human cancer cells. J Pharmacol Exp Ther 324: 95–102.

Takac I, Schroder K, Zhang L, Lardy B, Anilkumar N, Lambeth JD *et al.* (2011). The E-loop is involved in hydrogen peroxide formation by the NADPH oxidase Nox4. J Biol Chem 286: 13304–13313.

Takada Y, Mukhopadhyay A, Kundu GC, Mahabeleshwar GH, Singh S, Aggarwal BB (2003). Hydrogen peroxide activates NF-kappa B through tyrosine phosphorylation of I kappa B alpha and serine phosphorylation of p65: evidence for the involvement of I kappa B alpha kinase and Syk protein-tyrosine kinase. J Biol Chem 278: 24233–24241.

Thorens B, Mueckler M (2010). Glucose transporters in the 21st century. Am J Physiol Endocrinol Metab 298: E141–E145.

Trach P, Afahaene N, Nowak M, Thews O (2012). Impact of environmental parameters on the activity of the P-glycoprotein. Adv Exp Med Biol 737: 161–167.

van Uden P, Kenneth NS, Rocha S (2008). Regulation of hypoxia-inducible factor-1α by NF-κB. Biochem J 412: 477–484.

Walenta S, Schroeder T, Mueller-Klieser W (2002). Metabolic mapping with bioluminescence: basic and clinical relevance. Biomol Eng 18: 249–262.

Wang GL, Semenza GL (1993). Characterization of hypoxia-inducible factor 1 and regulation of DNA binding activity by hypoxia. J Biol Chem 268: 21513–21518.

Webb MS, Saxon D, Wong FMP, Lim HJ, Wang Z, Bally MB *et al.* (1998). Comparison of different hydrophobic anchors conjugated to poly(ethylene glycol): effects on the pharmacokinetics of liposomal vincristine. Biochim Biophys Acta 1372: 272–282.

Wei L, Dirksen RT (2012). Mitochondrial superoxide flashes: from discovery to new controversies. J Gen Physiol 139: 425–434.

Whitnall M, Howard J, Ponka P, Richardson DR (2006). A class of iron chelators with a wide spectrum of potent antitumor activity that overcomes resistance to chemotherapeutics. Proc Natl Acad Sci U S A 103: 14901–14906.

Yeom CJ, Goto Y, Zhu Y, Hiraoka M, Harada H (2012). Microenvironments and cellular characteristics in the micro tumor cords of malignant solid tumors. Int J Mol Sci 13: 13949–13965.

Yu T, Robotham JL, Yoon Y (2006). Increased production of reactive oxygen species in hyperglycemic conditions requires dynamic change of mitochondrial morphology. Proc Natl Acad Sci U S A 103: 2653–2658.

Yu T, Jhun BS, Yoon Y (2011). High-glucose stimulation increases reactive oxygen species production through the calcium and mitogen-activated protein kinase-mediated activation of mitochondrial fission. Antioxid Redox Signal 14: 425–437.

Zagzag D, Krishnamachary B, Yee H, Okuyama H, Chiriboga L, Ali MA *et al.* (2005). Stromal cell-derived factor-1α and CXCR4 expression in hemangioblastoma and clear cell-renal cell carcinoma: von Hippel-Lindau loss-of-function induces expression of a ligand and its receptor. Cancer Res 65: 6178–6188.

Zhong D, Liu X, Khuri FR, Sun S-Y, Vertino PM, Zhou W (2008). LKB1 is necessary for Akt-mediated phosphorylation of proapoptotic proteins. Cancer Res 68: 7270–7277.